A&A 372, 636–643 (2001)
DOI: 10.1051/0004-6361:20010509

Astronomy & Astrophysics

The radio spectral index of the Vela supernova remnant

H. Alvarez[1], J. Aparici[1], J. May[1], and P. Reich[2]

[1] Departamento de Astronomía, Universidad de Chile, Casilla 36-D, Santiago, Chile
[2] Max-Planck-Institut für Radioastronomie, Auf dem Hügel 69, 53121 Bonn, Germany

Received 25 October 2000 / Accepted 9 March 2001

Abstract. We have calculated the integrated flux densities of the different components of the Vela SNR between 30 and 8400 MHz. The calculations were done using the original brightness temperature maps found in the literature, a uniform criterion to select the background temperature, and a unique method to compute the integrated flux density. We have succeeded in obtaining separately, and for the first time, the spectrum of Vela Y and Vela Z. The index of the flux density spectrum of Vela X, Vela Y and Vela Z are -0.39, -0.70 and -0.81, respectively. We also present a map of brightness temperature spectral index over the region, between 408 and 2417 MHz. This shows a circular structure in which the spectrum steepens from the centre (Vela X) towards the periphery (Vela Y and Vela Z). X-ray observations show also a circular structure. We compare our spectral indices with those previously published.

Key words. ISM: supernova remnants – ISM: Vela X – radio continuum: ISM

1. Introduction

Radio continuum maps of the Vela SNR area show a complex structure. Three localized regions of enhanced brightness temperature stand out and have been defined by Rishbeth (1958) as Vela X, Vela Y and Vela Z; henceforth we will call them X, Y and Z, respectively. The most intense and well-defined is X; the other two are much weaker and blended. They lie on an arc to the north of X (see Fig. 1). The whole has been defined as XYZ. The intense supernova remnant (SNR) Puppis A is located in this area, and for this reason the complex has also been named Vela-Puppis. Vela-Puppis, covering about $5^\circ \times 5^\circ$, is within the large Gum Nebula area (about $10^\circ \times 10^\circ$) which, in addition to X, Y, Z and Puppis A, contains many other sources.

In order to establish the nature of the Vela SNR components, several authors have determined their spectral indices (e.g. Milne 1968, 1980; Weiler & Panagia 1980; Milne & Manchester 1986; Dwarakanath 1991). Because of Y and Z blending, only the indices of X and YZ have been published. The results obtained have stimulated a controversy between Milne et al. (Milne 1968; Milne & Manchester 1986) on one side, and Weiler et al. (Weiler & Panagia 1980; Weiler & Sramek 1988) on the other. Milne et al. have claimed that there is no significant difference between the indices of X and YZ ($\alpha \sim -0.35$) so that the whole Vela SNR belongs to the shell type. Weiler et al., on the other hand, sustain that YZ has a spectrum considerably steeper ($\alpha \sim -0.6$) than that of X ($\alpha \sim -0.1$), therefore X is a plerion while YZ belongs to the shell type SNR. The debate arose, to a large extent, from a lack of reliable measurements and also from confusion in the nomenclature of the components. Dwarakanath (1991) in detail presented the arguments of the controversy and attempted to resolve it.

The main purpose of this paper is to assess the distribution of radio spectral index over the Vela SNR from a reanalysis of published data.

Send offprint requests to: H. Alvarez,
e-mail: alvarez@das.uchile.cl

2. Results and discussion

2.1. Integrated flux densities

We will define α as the flux density spectral index ($S \propto \nu^\alpha$) and β the brightness temperature spectral index ($T \propto \nu^\beta$). The flux density will be implicitly assumed to be integrated flux density.

Three methods have been used in the literature to determine the flux density spectral index of an extended source. They rely on brightness temperature maps of the source, however not all of them are rigorously correct. The first method, and the only one strictly sound, integrates the temperature contours at each frequency and, taking care to remove the background temperature, directly

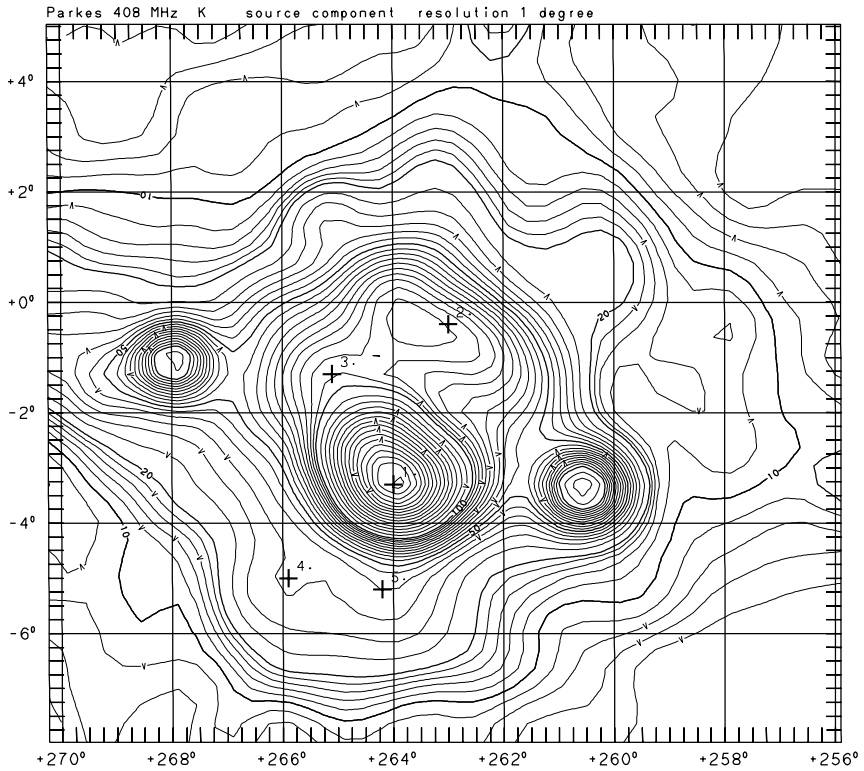

Fig. 1. Brightness temperature distribution of the Vela-Puppis area at 408 MHz smoothed to 1°. The position of the peaks of Vela X, Vela Y, Vela Z and the two peaks of Vela W, averaged from maps at different frequencies, are indicated by crosses numbered 1, 2, 3, 4 and 5, respectively. The source at $l = 268°$, $b = -1°$ is the HII region RCW 38. Puppis A is at $l = 261°$, $b = -3°$. The contours are labelled in K and the steps are 2 K up to 20 K, 5 K up to 100 K and 10 K further on. The galactic background has been removed.

calculates the integrated flux density. The second method consists of mapping the spatial distribution of β, derived usually from maps at only two frequencies and at the same resolution, and then computing α from the relationship $\alpha = \beta + 2$. When employed with care, this method may give a good approximation to the true value. We have found that only a few authors correctly discuss their results based on temperature indices. The third method assumes that some feature of the brightness temperature distribution (usually the peak value) bears some proportionality with the integrated flux density of the source. Unless the assumption is justified, the results are doubtful. Some authors have coined the term *peak flux density*. A peak flux density can be defined for an extended source if the source can be fitted to an elliptical Gaussian. The term *peak flux density* becomes meaningful when it is referred to as *peak flux density per beam area*.

The diversity of methods utilized to determine the spectral index of the Vela SNR components and the variety of results reached by different authors prompted us to redo the whole work. To that end we have determined the integrated flux densities of the classical X, Y and Z components by remeasuring the original brightness temperature maps used by previous workers between 29.9 and 8400 MHz, to which we have added one at 960 MHz (Wilson & Bolton 1960), and another at 2417 MHz (Duncan et al. 1995). We have estimated the background temperatures, which we have assumed to be the same for all three components at each frequency. In selecting the background temperatures we have also estimated the boundary (base contour) of the components. Until now the flux densities of Y and Z have not been measured separately, not only because they are much weaker than X but also because they are blended (See Fig. 1). Here we have attempted the separation by closing the temperature contours around them in a reasonable way. For each map we selected two possible base contours from which we obtained two possible background temperatures that were used to estimate the corresponding error. Since the components become weaker and less defined along the sequence X, Y and Z, the errors also increase likewise. The errors due to temperature calibrations are not usually given by the original authors and have not been included here. We expect that using a sufficient number of frequencies would reduce the corresponding error.

Table 1 presents the frequencies of the maps used, the two adopted background temperatures (T_1, T_2) and the references.

Some of the available maps were not considered for different reasons. Thus, the maps by Rishbeth (1958) at 19.7 and 85 MHz, by Mathewson et al. (1962) at 1440 MHz and by Alvarez et al. (1997) at 45 MHz do not have sufficient resolution, while the map by Jonas et al. (1998) at 2326 MHz is presented with too small a scale. Finally,

Table 1. Brightness temperature maps and base temperatures used to measure integrated flux densities.

ν (MHz)	T_1 (K)	T_2 (K)	Reference
29.9	44 100	38 220	Jones & Finlay (1974)
34.5	22 500	20 000	Dwarakanath (1991)
85.7	4000	3000	Hill et al. (1958)
408.0	60	50	Haslam et al. (1982)
635	10	5	Milne (1968)
960	1	0	Wilson & Bolton (1960)
1410	1	0	Milne (1968)
2417	1.4[a]	0.5[a]	Duncan et al. (1995)
2700	0.6	0.4	Day et al. (1972)
5000	0.2	0	Milne (1980)
8400	0.12[a]	0.09[a]	Milne (1995)

[a] Jy/beam area.

Table 2. Integrated flux densities measured in this work.

ν (MHz)	$S_{\mathrm{Vela}\,X}$ (Jy)	$S_{\mathrm{Vela}\,Y}$ (Jy)	$S_{\mathrm{Vela}\,Z}$ (Jy)	S_{XYZ}/S_{X+Y+Z}
29.9	3624 ± 390	3953 ± 563	3290 ± 475	0.73
34.5	1777 ± 183	1578 ± 178	1442 ± 158	0.91
85.7	2802 ± 606	1800 ± 398	1478 ± 422	1.16
408.0	2104 ± 211	980 ± 154	980 ± 234	1.07
635	1423 ± 137	435 ± 119	291 ± 98	0.93
960	1144 ± 189	588 ± 72	547 ± 83	0.70
1410	1162 ± 116	350 ± 86	258 ± 94	1.17
2417	843 ± 97	161 ± 13	96 ± 41	0.98
2700	815 ± 49	177 ± 65	100 ± 58	0.97
5000	567 ± 135			
8400	557 ± 54			

the map by Bock et al. (1998) at 843 MHz was not used because it misses angular features larger than about 1°.

Table 2 presents the integrated flux densities we measured for X, Y and Z. The 8400-MHz data, kindly provided by Dr. D. Milne, were re-processed by the method of unsharp masking (Sofue & Reich 1979) in order to remove remaining scanning effects.

As a test for the reliability of our measuring technique, we determined the integrated flux density of the HII regions RCW 36 and RCW 38. On the survey by Day et al. (1972), at 2700 MHz, these are seen as well-defined and rather intense sources, therefore the uncertainties of measurement should be small. The flux densities for RCW 36 and 38 given by Day et al. (1972) are 21 ± 1 and 290 Jy, while the values we have obtained are 19 ± 1 and 300 ± 15, respectively. We also measured the flux density of RCW 38 at 408 MHz and, using the base temperatures of Table 1, obtained 74 ± 16 Jy. This value and the 300 ± 15 Jy, found at 2700 MHz, fit well the spectrum given by Manchester & Goss (1969) between 85 and 5009 MHz.

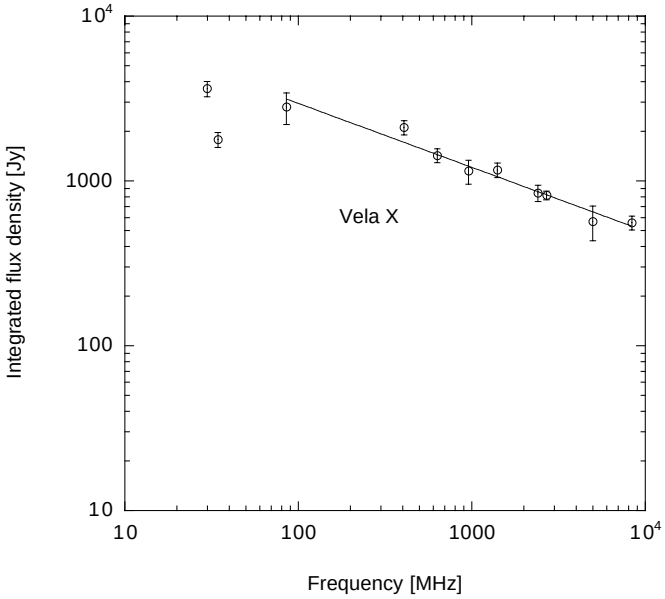

Fig. 2. Integrated flux density spectrum of Vela X. The straight line represents the least-squares fit to the data, given by the equation $\log S_{\mathrm{Vela}\,X} = (4.25 \pm 0.09) - (0.39 \pm 0.03) \log \nu$. The fit does not include the points at 29.9 and 34.4 MHz since they show some indication of absorption.

As a test for the internal consistency of our results we measured the integrated flux density of XYZ and compared it with that of $X + Y + Z$ by calculating the ratio $XYZ/(X + Y + Z)$. This comparison tests the choice of background temperatures and of the extension of the sources; in computing this ratio we have used only mean values, ignoring the errors. The results, presented in Table 2, indicate a reasonable self-consistency.

Figures 2–4 show the spectrum of X, Y and Z obtained with the values presented in Table 2. It is apparent that the uncertainties increase from X to Z.

2.2. Flux density spectral indices

In order to determine the spectral indices of X, Y and Z we need to do a linear fit to the flux densities presented in Table 2. The fluxes at 29.9 and 34.5 MHz are conflicting because, in spite of being close in frequency, they are significantly different, especially for X (where the errors are smaller). See Figs. 2–4. If the fit is made through all of the points at the different frequencies then the 34.5-MHz point appears too low with respect to the fit; on the other hand, if it is assumed that there is free-free absorption and the spectrum bends below about 85 MHz, then the 29.9-MHz point appears too high. Since we have found no reason to ignore one or the other of the fluxes we have adopted the criterion of excluding both from the linear fit. Thus, for X, Y and Z we have found the spectral indices of -0.39 ± 0.03, -0.70 ± 0.10, and -0.81 ± 0.16, respectively.

In Table 3 we compare our results for α_X with those from other authors. We see that Milne's indices are similar to ours but have a large uncertainty. This is to be

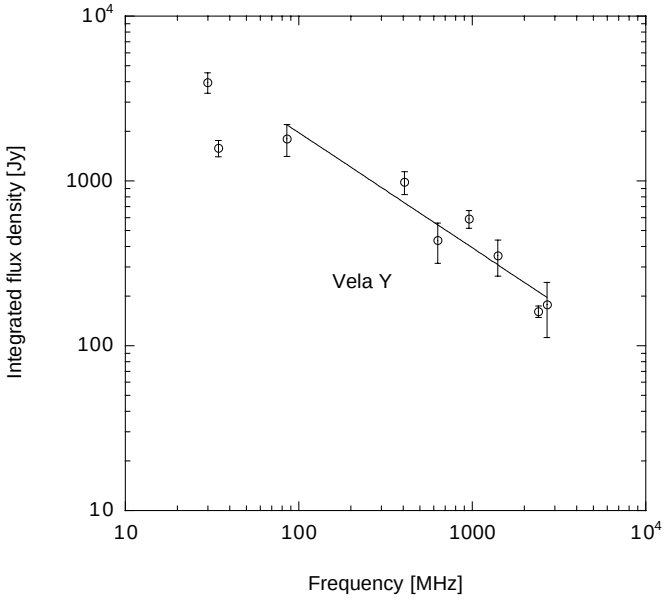

Fig. 3. Integrated flux density spectrum of Vela Y. The straight lines represent the least-squares fits to the data, given by the equation $\log S_{\mathrm{Vela}\,Y} = (4.69 \pm 0.29) - (0.70 \pm 0.10) \log \nu$. The fit does not include the points at 29.9 and 34.4 MHz since they show some indication of absorption.

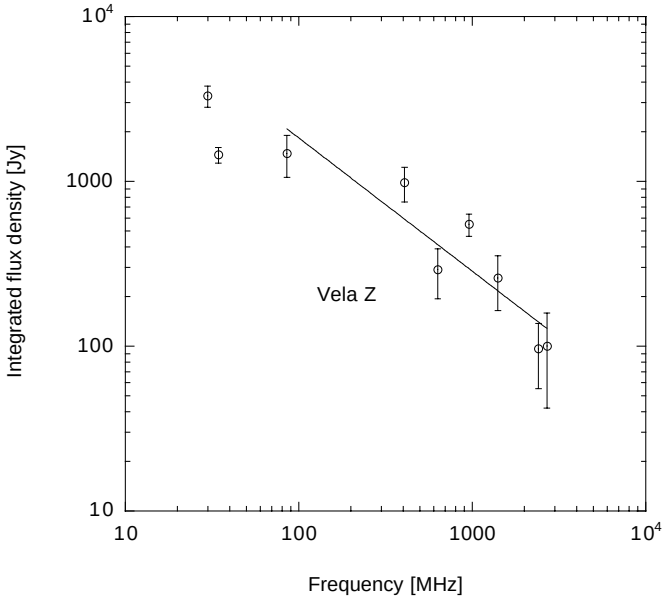

Fig. 4. Integrated flux density spectrum of Vela Z. The straight lines represent the least-squares fits to the data, given by the equation $\log S_{\mathrm{Vela}\,Z} = (4.88 \pm 0.47) - (0.81 \pm 0.16) \log \nu$. The fit does not include the points at 29.9 and 34.4 MHz since they show some indication of absorption.

expected since the error of β_X is assigned to α_X, which is a smaller number. The values of Weiler & Panagia, and of Dwarakanath are significantly larger than ours and Milne's; we take the results of these authors with caution because the former deduce integrated flux densities from the already discussed *peak full beam brightness temperatures*, while the latter uses data obtained through different criteria (see notes to Table 3).

In Table 4 we compare our results for Y and Z with those from other authors. Milne (1968) has given, with a large error, separate $\beta + 2$ values for these components, however there is no indication as to how the separation was done. It is significant, though, that the mean value is low (-0.6) and similar to the one we have determined. Later he adopted a value $\beta + 2 = -0.35 \pm 0.05$ for X, Y and Z (Milne & Manchester 1986). Weiler & Panagia (1980) and Dwarakanath (1991) have determined α_{YZ} (see notes [d] and [f] to Table 4), and they agree in the spectrum of YZ being steeper than X.

The notes to Tables 3 and 4 are intended to indicate the reliability of the determination based on the discussion made in Sect. 2.1. We believe our results for the indices of X, Y, and Z are more reliable than those of previous authors because they were obtained under advantageous conditions: first, from a homogeneous and self-consistent set of flux densities and, second, using the only strictly correct method, i.e., integrating the brightness temperature over the whole source.

We disagree with Milne et al. in that we find that α_Y and α_Z are lower than α_X, however we agree in that α_X is considerably lower than ~ -0.10. On the other hand, we disagree with Weiler et al. in that we find α_X considerably lower than ~ -0.10.

2.3. The morphology of the Vela SNR

Until now the Vela SNR has been assumed in the literature to be composed of X, Y and Z. While studying the extension of these components on the different maps we realized that there is a feature of intensified emission approximately south of X. It is even weaker than Y and Z and it has two peaks that can be clearly seen on the 29.9, 34.5 and 408 MHz (full-resolution) maps and, following the classical nomenclature, we have named it W (See Fig. 1). A very rough estimate of its flux density suggests that its spectrum is as steep as those of Y and Z. Duncan et al. (1996) and Bock et al. (1998) noticed this radiation at 2.4 GHz and 843 MHz, respectively, and suspected that it is a part of the Vela SNR; some other maps do not have a coverage large enough to show it. The approximate galactic coordinates (l, b) of the peaks of these features averaged on the different maps are (264.°0, $-3.°3$), (263.°0, $-0.°4$), (265.°1, $-1.°3$), (265.°9, $-5.°0$) and (264.°2, $-5.°2$) for X, Y, Z and the two peaks of W, respectively. The position of the peaks of Y, Z, and W suggests a circular symmetry around $l = 263.°6 \pm 0.°1$, $b = -3.°1 \pm 0.°1$. Such a circular structure has also been observed at X-rays by Aschenbach et al. (1995) and by Strom et al. (1995) who measured diameters of 8.°3 and 7.°3, respectively. They did not measure the position of the centre, but we have approximately determined it at $l = 263.°8$, $b = -2.°5$. Several authors have attempted to fit a circle through some of the Vela SNR

Table 3. Spectral index of Vela X.

α	$\beta+2$	ν (MHz)	Reference
$+0.0$[a]		19.7, 85.7, 960	Wilson (1963)
	-0.3 ± 0.2[b]	85–1440	Milne (1968)
	-0.4[c]	635, 1410, 2650	Milne (1968)
	-0.08 ± 0.02[d]	85.5–5000	Weiler & Panagia (1980)
	-0.35 ± 0.05[e]	408–2650	Milne & Manchester (1986)
-0.16 ± 0.02[f]		34.5–5000	Dwarakanath (1991)
	-0.10[g]	34.5, 408	Dwarakanath (1991)
-0.6 ± 0.2		2700, 5000, 8400	Milne (1995)
-0.39 ± 0.03		85.7–8400	This work

[a] Deduced from peak response assuming gaussian shapes. Data at 19.7 and 85.7 from Rishbeth (1958).
[b] Obtained by measuring only three points in the Vela XYZ region.
[c] Read by us from his Fig. 4.
[d] Deduced from peak full beam brightness temperatures.
[e] Not specified how it was obtained.
[f] The author uses: his observations at 34.5 MHz, Milne's data at 2700 and 5000 MHz, Rishbeth's data at 85 MHz, and his estimates at 19.7, 408 and 635 MHz.
[g] Read by us from his Fig. 6.

Table 4. Spectral index of Vela Y, Vela Z and Vela YZ.

$\alpha_{\mathrm{Vela}\,Y}$	$\beta_{\mathrm{Vela}\,Y}+2$	$\alpha_{\mathrm{Vela}\,Z}$	$\beta_{\mathrm{Vela}\,Z}+2$	$\alpha_{\mathrm{Vela}\,YZ}$	ν (MHz)	Reference
				-0.5[a]	19.7, 85.7, 960	Wilson (1963)
	-0.6 ± 0.4[b]		-0.6 ± 0.4[b]		85–1440	Milne (1968)
	-0.4[c]		-0.4[c]		635, 1410, 2650	Milne (1968)
				-0.65 ± 0.22[d]	408–2650	Weiler & Panagia (1980)
	-0.35 ± 0.05		-0.35 ± 0.05		408–2650	Milne & Manchester (1986)
	-0.45[e]		-0.5[e]		34.5, 408	Dwarakanath (1991)
				-0.53 ± 0.03[f]	34.5–2700	Dwarakanath (1991)
-0.70 ± 0.10		-0.81 ± 0.16			85.7–2700	This work

[a] From peak response assuming Gaussian shape. Data at 19.7 and 85.7 MHz are from Rishbeth (1958).
[b] Obtained by measuring only at three points in the Vela XYZ region. It is not explained how Vela Y and Vela Z were separated.
[c] Read by us from his Fig. 4.
[d] The fluxes of Vela YZ were obtained by subtracting the flux of Vela X from that of Vela XYZ. The flux of Vela X was deduced from peak full beam brightness temperature. The fluxes adopted for Vela XYZ were those by Milne (1968) and Harris (1962).
[e] Read by us from his Fig. 6.
[f] The 635 and 2700 MHz data were obtained by subtracting the flux of Vela X from that of Vela XYZ. The 2700 flux is said to be taken from Milne (1980, 1968), however these papers do not mention the flux density of this component. The 408 MHz flux is estimated from Haslam et al. (1982), while that at 635 MHz is estimated from Milne (1968).

components. For example, Duncan et al. (1996) fit an arc of circle to the northern part of the Vela SNR, locating the centre at $l=263\overset{\circ}{.}7$, $b=-3\overset{\circ}{.}2$, and estimating the diameter at $8\overset{\circ}{.}1\pm0\overset{\circ}{.}3$. Not unexpectedly, the centre is close to that of X and to the Vela pulsar located at $l=263\overset{\circ}{.}6$, $b=-2\overset{\circ}{.}8$. The component W is weakly present in their map and it was not considered. Manchester (1987) did the fitting in terms of two annular zones of emission and since the fit passed through X he necessarily obtained ovals. We have found no structure in the infrared between 12 and 100 micron images (Arendt 1989).

2.4. The spatial distribution of the temperature spectral index

In order to find independent support for the hypothesis that Y, Z, and W are physically associated, we have computed the spatial distribution of the brightness

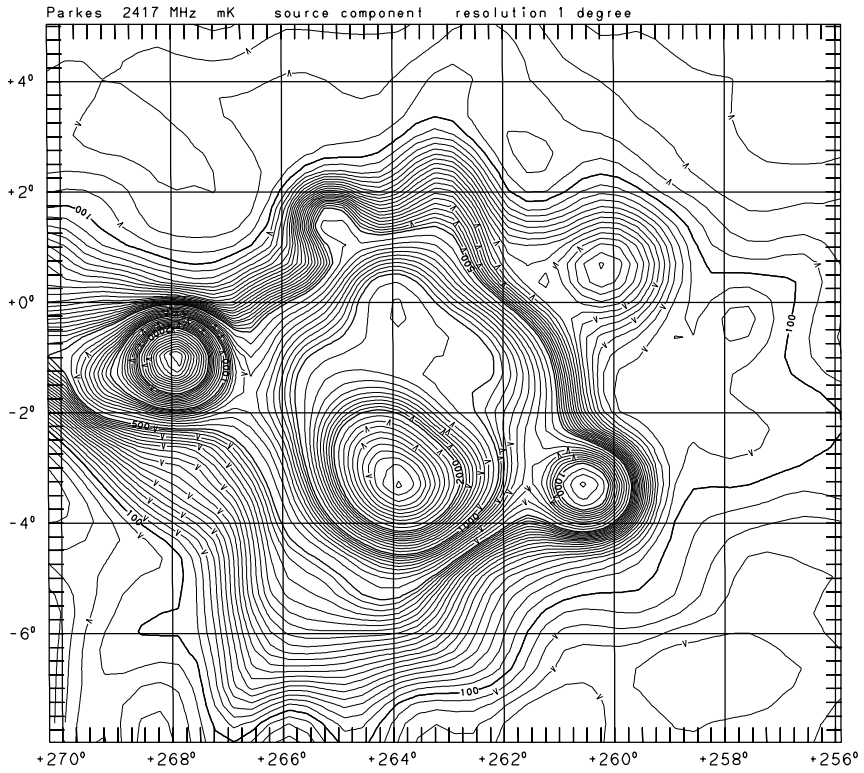

Fig. 5. Brightness temperature distribution at 2417 MHz, smoothed to a resolution of 1°. The contours are labelled in mK. The contour steps are 20 mK up to 500 mK, 50 mK up to 1 K, 100 mK up 2 K and 200 mK further on. The galactic background has been removed.

temperature spectral index between 408 and 2417 MHz, over the area surrounding the Vela SNR. The data, smoothed to 1° resolution, were those by Haslam et al. (1982) and by Duncan et al. (1995) at 408 and 2417 MHz, respectively. We have used the method of unsharp masking (Sofue & Reich 1979) to minimize some remaining scanning effects in the original 408-MHz data. We have also used this method to separate the data into a background and a source component at each frequency. The background was obtained by running 50 iterations with a filter beam of $300'(l) \times 100'(b)$. Figures 1 and 5 display the source component, with the background removed, at 408 MHz and 2417 MHz, respectively.

The spectral index map is shown in Fig. 6. We see that the distribution is circular and centered at X. There is a radial gradient with the maximum index $\beta \sim -2.3$ near the centre and decreasing to $\beta \sim -2.6$ near the periphery. The diameter of the circle outlining Vela SNR is $\sim 8°$. This distribution could be produced by a central source (X, $\beta \sim -2.3$) superimposed on a larger and uniform area with a steeper ($\beta \sim -2.6$) spectrum (YZW). We have tested this model by subtracting X and RCW 38 from the maps. The result shows, except for some residues, a circular area with a fairly constant spectral index ($\beta \sim -2.6$). In a three dimensional picture this circular area could be interpreted as a spherical shell or as a spherical filled volume.

In the literature we have found two maps of the $\beta + 2$ spatial distribution over the Vela SNR region. One by Milne (1968) covers only the X, Y and Z areas, and shows a distribution that resembles closely that of the brightness temperature. Three frequencies 635, 1410 and 2650 MHz were apparently used, and the data were convolved to $31'$. Values of $\beta + 2 \sim -0.4$ can be read at the peaks of the three features. The other map is by Dwarakanath (1991) and it covers all the Vela SNR region. The spectral index was computed using 34.5 and 408 MHz, and the data were smoothed to $1° \times 1.°5$. The approximate $\beta + 2$ at the positions of the peaks of X, Y and Z are -0.15, -0.41, and -0.47, respectively, while the distribution does not resemble either a ring or any closed figure. The indices determined by Dwarakanath (1991, see his Fig. 6) are systematically larger than ours. We believe this is because his data at 34.5 MHz is most likely affected by absorption. In fact Milne & Manchester (1986) find evidence for absorption at 85 MHz. On another map Milne (1980) shows the distribution of β, however, over the X area only. He calculated the spectral index from 2.7 and 5.0 GHz, with a resolution of about $9'$. At this high resolution, large fluctuations, between -1.8 and -3.0, are seen, which emphasizes the conceptual difference between the indices α and β.

3. Conclusions

We have studied the Vela SNR region, reaching the following conclusions:

1. Following common practice we have assumed Vela X, Vela Y and Vela Z to be individual sources and

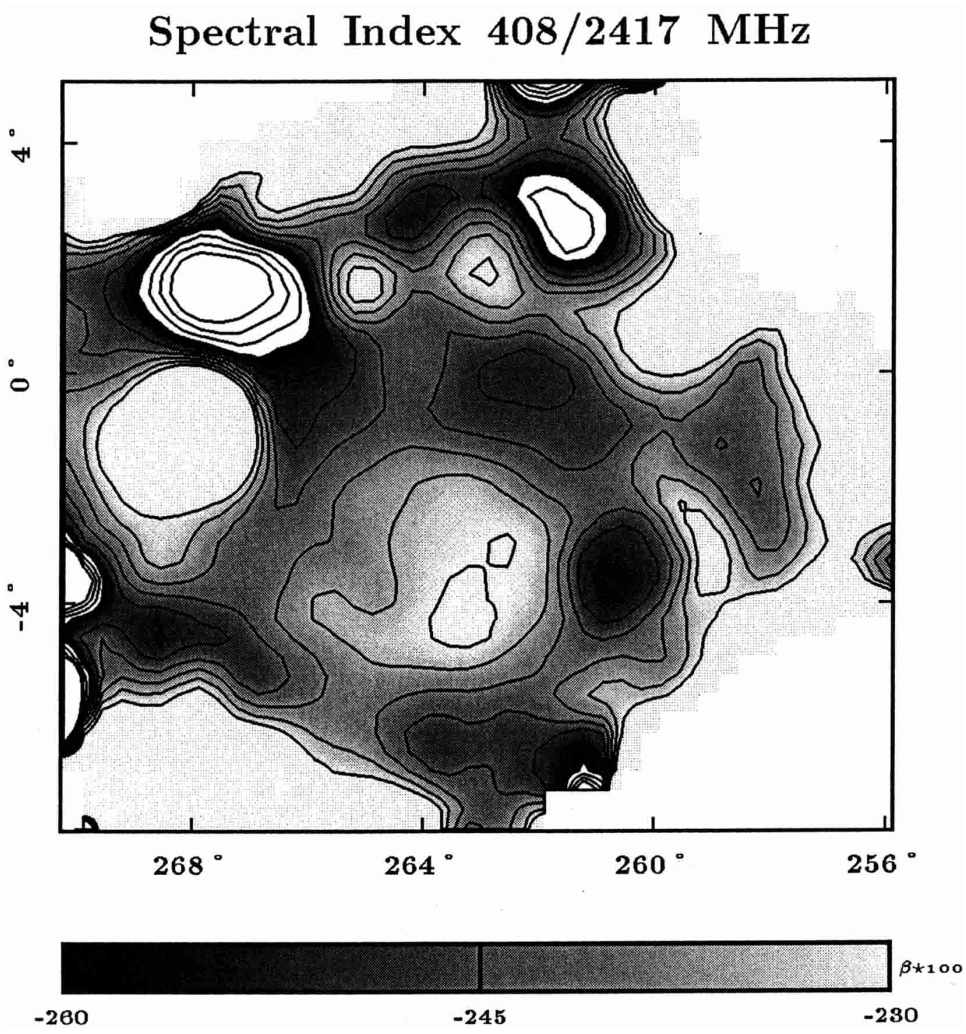

Fig. 6. Brightness temperature spectral index (408/2417 MHz) over the Vela-Puppis area. The map shows a circular distribution around Vela X ($264\overset{\circ}{.}0, -3\overset{\circ}{.}3$). This structure can de produced by a source with index $\beta \sim -2.3$, at the centre, superimposed on a larger circular area with a steeper ($\beta \sim -2.6$) and uniform spectrum. The source at ($268°$, $-1°$) is the HII region RCW 38. The gray scale starts at $\beta = -2.3$ (white) and runs to $\beta = -2.6$ (black). The contours start at -2.3 in steps of -0.05.

we have measured their integrated flux densities using brightness temperature maps available in the literature. These measurements, made with the same method and the same criterion for all the components, at nine or ten frequencies, have provided a unique homogeneous and self-consistent set of data. The flux indices we have found are: $\alpha_X = -0.39 \pm 0.03$, between 85.7 and 8400 MHz, and $\alpha_Y = -0.70 \pm 0.10$ and $\alpha_Z = -0.81 \pm 0.16$, between 85.7 and 2700 MHz. The integrated flux density spectrum of Vela Y and Vela Z we have presented have been measured separately, for the first time;

2. We have presented a map of the spatial distribution of the temperature spectral index (408/2417 MHz) over the Vela SNR area that shows a circular symmetry of the Vela SNR. The index exhibits a radial gradient such that the steepness of the spectrum increases from the centre towards the periphery. We have shown that this distribution is consistent with the hypothesis that the Vela SNR has a spherical geometry, most likely a shell, with a fairly constant spectral index, over which is superimposed the less steep spectrum of Vela X, located at the centre.

Acknowledgements. We are grateful to Dr. D. K. Milne for providing the original 8.4 GHz data of Vela X, and to Dr. W. Reich for critically reading the manuscript. We thank an anonymous referee whose useful comments improved the paper. This research has been supported by FONDECYT through grant 8970017.

References

Alvarez, H., Aparici, J., May, J., & Olmos, F. 1997, A&AS, 124, 315

Aschenbach, B., Egger, R., & Trumper, J. 1995, Nature, 373, 587

Bock, D. C.-J., Turtle, A. J., & Green, A. J. 1998, ApJ, 116, 1886
Day, G. A., Caswell, J. L., & Cooke, D. J. 1972, Aust. J. Phys. Astrophys. Suppl., 25
Duncan, A. R., Stewart, R. T., Haynes, R. F., & Jones, K. L. 1995, MNRAS, 277, 36
Duncan, A. R., Stewart, R. T., Haynes, R. F., & Jones, K. L. 1996, MNRAS, 280, 252
Dwarakanath, K. S. 1991, JA&A, 12, 199
Haslam, C. G. T, Salter, C. J., Stoffel, H., & Wilson, W. E. 1982, A&AS, 47, 1
Hill, E. R., Slee, O. B., & Mills, B. Y. 1958, Aust. J. Phys., 11, 530
Jonas, J. L., Baart, E. E., & Nicolson, G. D. 1998, MNRAS, 297, 977
Jones, B. B., & Finlay, E. A. 1974, Aust. J. Phys., 27, 687
Manchester, R. N. 1987, A&A, 171, 205
Manchester, B. A., & Goss, W. M. 1969, Aust. J. Phys. Astrophys. Suppl., 11, 35
Mathewson, D. S., Healey, J. R., & Rome, J. M. 1962, Aust. J. Phys., 15, 345
Milne, D. K. 1968, Aust. J. Phys., 21, 201
Milne, D. K. 1980, A&A, 81, 293
Milne, D. K. 1995, MNRAS, 277, 1435
Milne, D. K., & Manchester, R. N. 1986, A&A, 167, 117
Rishbeth, H. 1958, Aust. J. Phys., 11, 550
Sofue, Y., & Reich, W. 1979, A&AS, 38, 251
Strom, R., Johnston, H. M., Verbunt, F., & Aschenbach, B. 1995, Nature, 373, 590
Weiler, K. W., & Panagia, N. 1980, A&A, 90, 269
Weiler, K. W., & Sramek, R. A. 1988, ARA&A, 26, 295
Wilson, R. W. 1963, AJ, 68, 181
Wilson, R. W., & Bolton, J. G. 1960, PASP, 72, 331